

# Source radii at target rapidity from two-proton and two-deuteron correlations in central Pb+Pb collisions at 158 A GeV

WA98 Collaboration

M.M. Aggarwal<sup>1</sup>, Z. Ahammed<sup>2</sup>, A.L.S. Angelis<sup>3,\*</sup>, V. Antonenko<sup>4</sup>, V. Arefiev<sup>5</sup>, V. Astakhov<sup>5</sup>, V. Avdeitchikov<sup>5</sup>, T.C. Awes<sup>6</sup>, P.V.K.S. Baba<sup>7</sup>, S.K. Badyal<sup>7</sup>, S. Bathe<sup>8</sup>, B. Batiounia<sup>5</sup>, T. Bernier<sup>9</sup>, K.B. Bhalla<sup>10</sup>, V.S. Bhatia<sup>1</sup>, C. Blume<sup>8</sup>, D. Bucher<sup>8</sup>, H. Büsching<sup>8</sup>, L. Carlen<sup>11</sup>, S. Chattopadhyay<sup>2</sup>, M.P. Decowski<sup>12</sup>, H. Delagrange<sup>9</sup>, P. Donni<sup>3</sup>, M.R. Dutta Majumdar<sup>2</sup>, K. El Chenawi<sup>11</sup>, A.K. Dubey<sup>13</sup>, K. Enosawa<sup>14</sup>, S. Fokin<sup>4</sup>, V. Frolov<sup>5</sup>, M.S. Ganti<sup>2</sup>, S. Garpman<sup>11,\*</sup>, O. Gavrishchuk<sup>5</sup>, F.J.M. Geurts<sup>15</sup>, T.K. Ghosh<sup>16</sup>, R. Glasow<sup>8</sup>, B. Guskov<sup>5</sup>, H. Å.Gustafsson<sup>11</sup>, H. H.Gutbrod<sup>17</sup>, I. Hrivnacova<sup>18</sup>, M. Ippolitov<sup>4</sup>, H. Kalechofsky<sup>3</sup>, R. Kamermans<sup>15</sup>, K. Karadjev<sup>4</sup>, K. Karpio<sup>19</sup>, B. W. Kolb<sup>17</sup>, I. Kosarev<sup>5</sup>, I. Koutcheryaev<sup>4</sup>, A. Kugler<sup>18</sup>, P. Kulnich<sup>12</sup>, M. Kurata<sup>14</sup>, A. Lebedev<sup>4</sup>, H. Liu<sup>19</sup>, H. Löhner<sup>16</sup>, L. Luquin<sup>9</sup>, D.P. Mahapatra<sup>13</sup>, V. Manko<sup>4</sup>, M. Martin<sup>3</sup>, G. Martínez<sup>9</sup>, A. Maximov<sup>5</sup> and Y. Miake<sup>14</sup>, G.C. Mishra<sup>13</sup>, B. Mohanty<sup>13</sup>, M.-J. Mora<sup>9</sup>, D. Morrison<sup>20</sup>, T. Moukhanova<sup>4</sup>, D. S. Mukhopadhyay<sup>2</sup>, H. Naef<sup>3</sup>, B. K. Nandi<sup>13</sup>, S. K. Nayak<sup>9</sup>, T. K. Nayak<sup>2</sup>, A. Nianine<sup>4</sup>, V. Nikitine<sup>5</sup>, S. Nikolaev<sup>4</sup>, P. Nilsson<sup>11</sup>, S. Nishimura<sup>14</sup>, P. Nomokonov<sup>5</sup>, J. Nystrand<sup>11</sup>, A. Oskarsson<sup>11</sup>, I. Otterlund<sup>11</sup>, S. Pavliouk<sup>4</sup>, T. Peitzmann<sup>15</sup>, D. Peressouko<sup>4</sup>, V. Petracek<sup>18</sup>, V. Petracek<sup>13</sup>, W. Pinanaud<sup>9</sup>, F. Plasil<sup>6</sup>, M.L. Purschke<sup>17</sup>, J. Rak<sup>18</sup>, R. Raniwala<sup>10</sup>, S. Raniwala<sup>10</sup>, N.K. Rao<sup>7</sup>, F. Retiere<sup>9</sup>, K. Reygers<sup>8</sup>, G. Roland<sup>12</sup>, L. Rosselet<sup>3</sup>, I. Roufanov<sup>5</sup>, C. Roy<sup>9</sup>, J.M. Rubio<sup>3</sup>, S.S. Sambyal<sup>7</sup>, R. Santo<sup>8</sup>, S. Sato<sup>14</sup>, H. Schlagheck<sup>8</sup>, H.-R. Schmidt<sup>17</sup>, Y. Schutz<sup>9</sup>, G. Shabratova<sup>5</sup>, T.H. Shah<sup>7</sup>, I. Sibiriak<sup>4</sup>, T. Siemiarczuk<sup>19</sup>, D. Silvermyr<sup>11</sup>, B.C. Sinha<sup>2</sup>, N. Slavine<sup>5</sup>, K. Söderström<sup>11</sup>, G. Sood<sup>1</sup>, S.P. Sørensen<sup>20</sup>, P. Stankus<sup>6</sup>, G. Stefanek<sup>19</sup>, P. Steinberg<sup>12</sup>, E. Stenlund<sup>11</sup>, M. Sumbera<sup>18</sup>, T. Svensson<sup>11</sup>, A. Tsvetkov<sup>4</sup>, L. Tykarski<sup>19</sup>, E.C.v.d. Pijll<sup>15</sup>, N.v. Eijndhoven<sup>15</sup>, G.J.v. Nieuwenhuizen<sup>12</sup>, A. Vinogradov<sup>4</sup>, Y.P. Viyogi<sup>2</sup>, A. Vodopianov<sup>5</sup>, S. Vörös<sup>3</sup>, B. Wyslouch<sup>12</sup>, and G.R. Young<sup>6</sup>

<sup>1</sup> University of Panjab, Chandigarh 160014, India

<sup>2</sup> Variable Energy Cyclotron Centre, Calcutta 700 064, India

<sup>3</sup> University of Geneva, CH-1211 Geneva 4, Switzerland

<sup>4</sup> RRC Kurchatov Institute, RU-123182 Moscow, Russia

<sup>5</sup> Joint Institute for Nuclear Research, RU-141980 Dubna, Russia

<sup>6</sup> Oak Ridge National Laboratory, Oak Ridge, Tennessee 37831-6372, USA

<sup>7</sup> University of Jammu, Jammu 180001, India

<sup>8</sup> University of Münster, D-48149 Münster, Germany

<sup>9</sup> SUBATECH, Ecole des Mines, Nantes, France

<sup>10</sup> University of Rajasthan, Jaipur 302004, Rajasthan, India

<sup>11</sup> Lund University, SE-221 00 Lund, Sweden

<sup>12</sup> MIT Cambridge, MA 02139, USA

<sup>13</sup> Institute of Physics, 751-005 Bhubaneswar, India

<sup>14</sup> University of Tsukuba, Ibaraki 305, Japan

<sup>15</sup> Universiteit Utrecht/NIKHEF, NL-3508 TA Utrecht, The Netherlands

<sup>16</sup> KVI, University of Groningen, NL-9747 AA Groningen, The Netherlands

<sup>17</sup> Gesellschaft für Schwerionenforschung (GSI), D-64220 Darmstadt, Germany

<sup>18</sup> Nuclear Physics Institute, CZ-250 68 Rez, Czech Rep.

<sup>19</sup> Soltan Institute for Nuclear Studies, PL-00-681 Warsaw, Poland

<sup>20</sup> University of Tennessee, Knoxville, Tennessee 37966, USA

\* Deceased.

Received: date / Revised version: date

**Abstract.** Two-proton and two-deuteron correlations have been studied in the target fragmentation region of central Pb+Pb collisions at 158 A GeV. Protons and deuterons were measured with the Plastic Ball spectrometer of the WA98 experiment at the CERN SPS. The results of one-dimensional and multi-dimensional analyses using both the Bertsch-Pratt and Yano-Koonin-Podgoretsky parameterizations of the two-particle correlation functions are presented. The proton source exhibits a volume emission, while the deuteron source, with small outward radius, appears opaque. Both proton and deuteron sources have cross-terms  $R_{ol}^2$  and longitudinal velocities  $\beta$  consistent with zero, indicat-

ing a boost-invariant expansion. The invariant radius parameter  $R$  follows an approximate  $A/\sqrt{m}$  scaling while the longitudinal and transverse radii,  $R_L$  and  $R_T$ , scale approximately as  $A/\sqrt{m_T}$  with  $A \approx 3 \text{ fm GeV}^{1/2}$  in both cases.

**PACS.** 25.75. Gz

## 1 Introduction

In this paper we report on an analysis of quantum-statistical and final state induced correlations [1] of proton and deuteron pairs emitted from 158 A GeV central Pb+Pb collisions. The study of these two particle species in the same system is of special interest as one would expect that deuterons, due to their loose structure and small binding energy, will survive only in the late, low density environment when scatterings are rare. The generally accepted mechanism of deuteron production is by coalescence of a proton and neutron [2,3,4] at the time of freeze-out. The deuteron measurement thus provides a unique means to measure the geometry of the source in the late time interval of the expansion. Experimental results on Fermi-Dirac correlations for protons are not as abundant as those on Bose-Einstein correlations for mesons, and are very scarce for deuteron correlations. A remarkable feature of the existing proton and deuteron correlation data in hadron-nucleus and nucleus-nucleus collisions, spanning over four orders of magnitude of incident energy from 0.02 to 450 A GeV is the small variation of the extracted source radius parameter [5,6,7,8,9,10,11,12,13,14,15,16,17,18,19,20,21].

## 2 Experimental setup

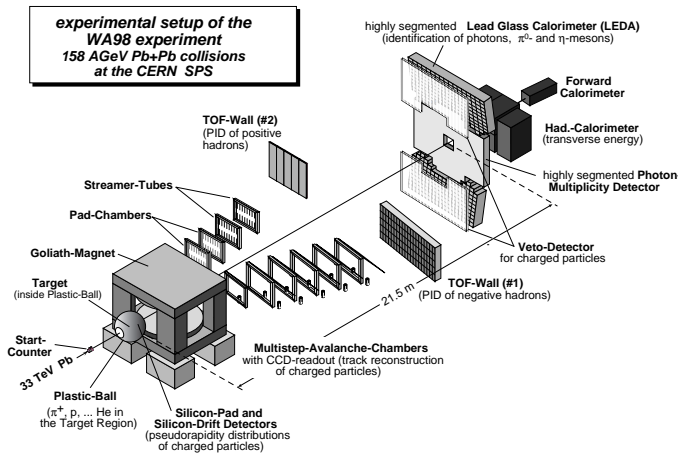


Fig. 1. Experimental setup of the WA98 experiment for the 1996 run.

The CERN SPS experiment WA98 (for details see [22] and references therein) is a general purpose apparatus that consists of large acceptance photon and hadron spectrometers, detectors for charged particle and photon multiplicity measurements, and calorimeters for transverse and forward energy measurements. The layout of the WA98 experimental setup for the 1996 SPS run period is shown in Fig. 1. The results presented in this report were obtained from an analysis of data taken in 1996 with the 158 A GeV  $^{208}\text{Pb}$  beam on a  $239 \text{ mg/cm}^2$   $^{208}\text{Pb}$  target

and made use of the Midrapidity Calorimeter (MIRAC) [23], the Zero Degree Calorimeter (ZDC) [24], and the Plastic Ball spectrometer [25].

The ZDC registers energy emitted along the beam direction in the  $3^\circ$  forward cone. The MIRAC measures the total transverse energy in the pseudorapidity region of  $3.5 \leq \eta \leq 5.5$ . It is a sampling calorimeter that consists of a lead-scintillator electromagnetic section, followed by an iron-scintillator hadronic section. MIRAC plays the central role in the WA98 minimum bias trigger where the measured transverse energy  $E_T$  is required to be above a minimum threshold. MIRAC is used to classify the centrality of each event. The analysis presented here has been performed on the 10% most central events of the measured minimum bias cross section of  $\approx 6400 \text{ mb}$ . About 3 millions central Pb+Pb events were analyzed with an average of 6.1 identified protons and 2.9 identified deuterons per event.

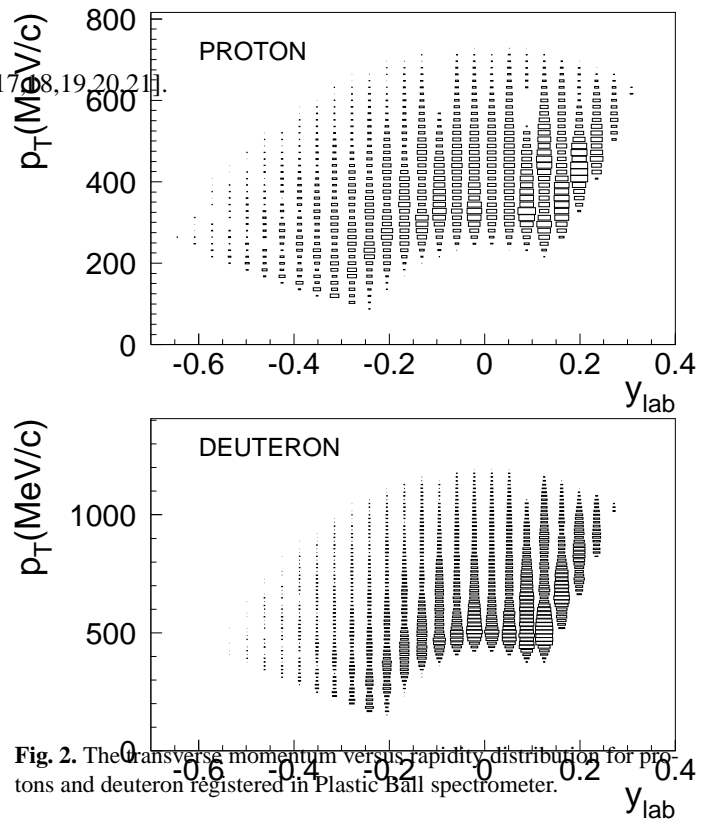


Fig. 2. The transverse momentum versus rapidity distribution for protons and deuteron registered in Plastic Ball spectrometer.

The identification and momentum measurement of protons and deuterons has been made using the Plastic Ball spectrometer [25]. The Plastic Ball consists of 655 detector modules surrounding the target over the range of polar angles  $\vartheta$  from  $30^\circ$  to  $160^\circ$  with full azimuthal acceptance. Each of the modules consists of a  $\Delta E$  and  $E$  section. The  $\Delta E$  section is a  $\text{CaF}_2(\text{Eu})$  crystal scintillator and the  $E$  section is a plastic scintillator. The light emission of the plastic scintillator is approximately 100

times faster than that of the  $\text{CaF}_2(\text{Eu})$ , so signals from both scintillators can be read out by a single photomultiplier with subsequent separation of the signals by pulse shape analysis. The  $\Delta E - E$  identification technique was used and is capable of identifying pions and charged fragments up to the helium isotopes. Because of the relatively low yield of pions as compared to baryons, an additional positive pion identification is made by means of its sequential decay  $\pi^+ \rightarrow \mu^+(\nu_\mu) \rightarrow e^+(\nu_e \bar{\nu}_\mu)$ . The thickness of the  $\Delta E$  crystal scintillator was chosen to be 4 mm with 35.6 cm as the length of the  $E$  plastic scintillator. This assures that protons up to 200 MeV are fully stopped in the  $E$ -counter and provide a complete  $\Delta E - E$  signal. Additionally, the mis-identification of punch through deuterons do not disturb the proton spectra below 200 MeV.

The WA98 experimental setup has been implemented in the GEANT Monte Carlo simulation package [26]. This has been used to study the response of the Plastic Ball in order to extract the particle identification efficiency and the kinetic energy resolution for different particle species, as well as two-particle variables and takes into account the granular structure of the Plastic Ball. GEANT transports the particles through the experimental setup taking into account the geometrical material boundaries and particle interactions. The particles are traced through the experimental setup where they may interact with the material they encounter on their way to the detector. When a particle reaches the detector the output signal of the Plastic Ball module is simulated. The particle distributions used as input to the GEANT simulations were adjusted to reproduce the measured momentum and angular distributions of particles. The Plastic Ball acceptance is illustrated in Fig. 2 as the distribution of protons and deuterons that pass the acceptance cuts.

### 3 One-dimensional analysis

The one-dimensional experimental correlation function was constructed as:

$$C(q) = N \frac{Y_{12}(q)}{Y_{12}^*(q)} \quad (1)$$

where  $\mathbf{q} = \frac{1}{2}(\mathbf{q}_1 - \mathbf{q}_2)$  is the two-particle three-momentum difference in the laboratory frame,  $N$  is a normalization constant, and the numerator is the coincidence yield while the denominator is the uncorrelated background yield. In this analysis, the event-mixing technique was used to construct the background yields, using the same central event data set as used to construct the numerator. To insure that only particles from comparable events were mixed, the central event sample was further subdivided into 8 subsets according to the measured transverse energy. Particles were picked randomly from different events belonging to the same centrality selection with the additional condition to have the same multiplicities of the studied particle and all particles registered in the Plastic Ball. The number of mixed background pairs was chosen to be 10 times larger than the number of coincident pairs to insure a small statistical error contribution from the background pair yield,  $Y_{12}^*$ .

The measurement resolution of the variable  $q$  in the Plastic Ball spectrometer had an average value of  $\sigma(q) \simeq 10.5$  MeV/c and 12.5 MeV/c for the two-proton and two-deuteron systems, respectively. For small values of  $q$ , the resolution was

around 7.5 MeV/c for the two-proton system. A bin size of 7.5 MeV/c was chosen for the one-dimensional correlation analyses. It should be noted that the one-dimensional correlation functions presented here have been studied as a function of the momentum difference  $q$  rather than the more commonly used invariant four-momentum difference  $q_{inv} = \frac{1}{2} \sqrt{-(p_1^\mu - p_2^\mu)^2}$ . The experimental resolution for the pp (dd) system in  $q_{inv}$  at 20 (40) MeV/c is about 15 (20) MeV/c. It increases to 20 (27) MeV/c at  $q_{inv}=100$  (200) MeV/c and approximately levels off above that.

#### 3.1 Final state interaction

To calculate the pair-wise final state interaction we used two computer codes for the proton-proton system: (i) the CRAB code written by S.Pratt [27] which includes Coulomb and strong final state interactions, and (ii) the static model developed by A. Deloff [28,29] with both Coulomb and strong S-wave interactions included. The latter incorporates a potential of the delta-shell form

$$2\mu V(r) = -(s/R) \delta(r - R), \quad (2)$$

characterized by the range  $R$  and the dimensionless parameter  $s$  representing the strength of the force ( $\mu$  is the reduced mass). Only the  $^1S_0$  partial wave in the strong interaction was retained. This pp interaction is well known experimentally and the measured phase shifts can be satisfactorily reproduced up to  $q=150$  MeV/c by taking the delta-shell potential parameters as  $s=0.906$  and  $R=1.84$  fm. Both codes gave consistent results for the proton-proton system.

For the deuteron-deuteron case the model by A. Deloff [28] was used in which the strong s-wave interaction in  $S=0,2$  spin states was included together with the Coulomb repulsion between two extended-size deuterons. The Coulomb interaction between two deuterons is different from that between two protons because the deuteron is composite and relatively large. For two extended-size deuterons located at  $\mathbf{r}_1$  and  $\mathbf{r}_2$ , the Coulomb potential can be written as

$$V(|\mathbf{r}_1 - \mathbf{r}_2|) = \alpha \int d^3\mathbf{x}_1 d^3\mathbf{x}_2 \frac{\rho(|\mathbf{x}_1 - \mathbf{r}_1|) \rho(|\mathbf{x}_2 - \mathbf{r}_2|)}{|\mathbf{x}_1 - \mathbf{x}_2|} \quad (3)$$

where  $\rho(x)$  is the charge density and  $\alpha$  is the fine structure constant. Since the right hand side of Eq. (3) is translationally invariant, the potential  $V(r)$  depends only upon the difference  $r = |\mathbf{r}_1 - \mathbf{r}_2|$ , and for  $r$  larger than twice the deuteron radius takes the usual point-like form  $V(r) = \alpha/r$ . For an assumed uniform charge distribution, this integral can be obtained in analytic form as:

$$V(r) = \begin{cases} \frac{\alpha}{R_c} \frac{1}{x} \{1 - 3(1-x)^4 \\ \times [1 - \frac{2}{15}(1-x)(5+x)]\} & 0 \leq x \leq 1 \\ \frac{\alpha}{r} & x > 1 \end{cases} \quad (4)$$

where  $x = r/R_c$  and  $R_c = 3.86$  fm is twice the deuteron radius. A comparison of the Coulomb potential for extended-size and point-like deuterons is shown in Fig. 3. The Coulomb repulsion is observed to be substantially reduced when the extended deuteron size is taken into account.

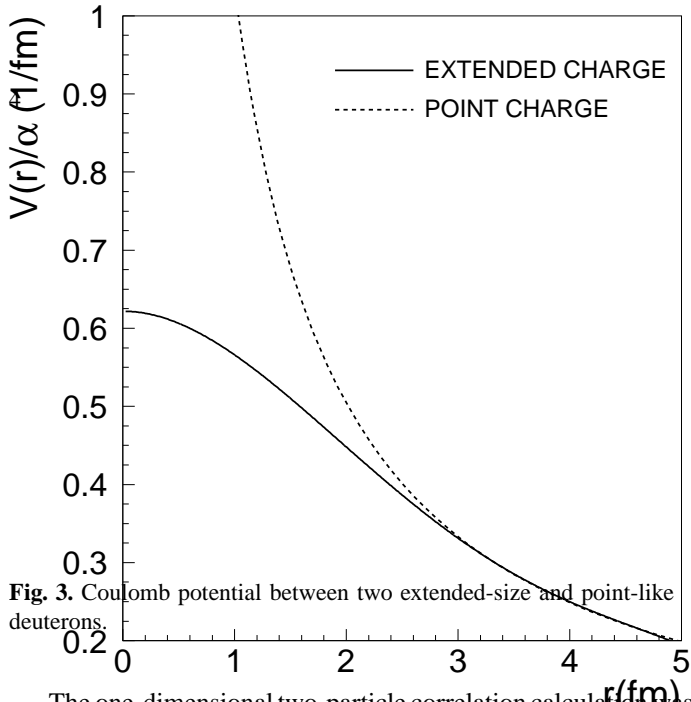


Fig. 3. Coulomb potential between two extended-size and point-like deuterons.

The one-dimensional two-particle correlation calculation was based on a static spherical gaussian shaped source, specified by radius  $R_0$ :

$$\rho(x) = (2\pi R_0^2)^{-3/2} e^{-x^2/2R_0^2}. \quad (5)$$

In the case of a non-zero emission lifetime this approach gives an *upper* limit for the spatial extent of the source.

To account for the Plastic Ball resolution all of the calculated correlation functions presented in this paper were calculated as:

$$C(q) = \int r(q, q') C(q') dq' \quad (6)$$

with the predicted correlation function  $C(q')$  convoluted with the Gaussian resolution function of the Plastic Ball  $r(q, q')$ .

$$r(q, q') = \frac{1}{(2\pi)^{3/2}} \frac{1}{\sigma(q)} e^{-\frac{1}{2} \frac{(q-q')^2}{\sigma(q)^2}} dq' \quad (7)$$

as determined from the GEANT simulations.

### 3.2 Systematic errors

The systematic errors have been evaluated by comparison of the results obtained under different conditions. The systematic uncertainties are mainly introduced by the granularity of the detector and, to some extent, by the procedure used to construct the background pair distribution. The following sources of systematic errors have been investigated leading to variations (rms estimates) of the radius parameters given in brackets, with the first and second numbers referring to the pp and dd system, respectively:

- (i) Different periods of data taking during the run [0.05, 0.05 fm].
- (ii) Different particle identification windows [0.09, 0.12 fm].
- (iii) The width of the transverse energy  $E_T$  bin used for centrality selection in the background pair distribution calculations: the centrality bin size was halved and the result was compared to the nominal bin size result [0.01, 0.05 fm].

- (iv) Non-conservation of momentum in the background pair correlations: local (transverse) momentum conservation in real events, although not expected to be exact, may influence the correlation between real particle pairs due to the fact that a significant fraction, but not all, of the particles in the target rapidity region are measured in the Plastic Ball. To investigate the sensitivity of the fitted parameters to the effect of momentum conservation, in addition to the requirement that the full background event have the same number of particles as the real event detected in the Plastic Ball, it was further required that the background event have a total momentum of all measured particles equal to that of the real event:  $P_{Tot}(\text{measured}) = P_{Tot}(\text{reference}) \pm \Delta$ , where  $\Delta$  should be 0 in the ideal case. In practice,  $\Delta$  was chosen to be 300 MeV/c and 600 MeV/c for the two-proton and two-deuteron background events, respectively [0.07, 0.06 fm].
- (v) The granular structure of the Plastic Ball spectrometer: the GEANT program has been used to study the distortion of the correlation function due to the granularity of the Plastic Ball detector [0.15, 0.10 fm].
- (vi) The bin width of the correlation function: to examine the dependence of the radius parameters on the  $q$  bin width, the analysis was also performed with bin widths of 10 MeV/c and 5 MeV/c [0.06, 0.06 fm].
- (vii) Detector variation: the analysis was performed separately in two different azimuthal angle intervals:  $0^\circ - 180^\circ$  and  $180^\circ - 360^\circ$  [0.01, 0.02 fm].
- (viii) The effect of possible mis-identification of protons and deuterons due to the multiple hits to the same Plastic Ball module. Since the multi-hit probability depends very strongly on  $\theta$ , the analysis was performed with two subsamples with  $\theta$  intervals of protons and deuterons:  $60^\circ - 90^\circ$  and  $90^\circ - 160^\circ$ . The ratio of contaminations due to multi-hits in these  $\theta$  intervals is about 10:1. The GEANT simulations also demonstrated that the contamination from spurious protons and deuterons contribute uniformly to their correlation functions. As a result, this background contamination does not affect the shape of the correlation function, leading to the same, within errors, radius parameters [0.15, 0.10 fm].

The total systematic uncertainty was calculated by adding in quadrature the contributions listed above.

### 3.3 Two-proton system

The measured two-proton correlation function is shown in Fig. 4. The solid line represents the result of the theoretical calculation which gives the best fit to the data using the delta-shell potential. The final state Coulomb and strong interactions, the Fermi-Dirac effect, and the experimental resolution have been implemented in the theoretical calculation. The resulting radius parameter is  $3.14 \pm 0.03(\text{stat.}) \pm 0.21(\text{syst.})$  fm.

Although the delta-shell potential may not be realistic, its main advantage is that both the phase shift and the enhancement factor can be obtained in an analytic form. Furthermore, it is desirable to use the same model for calculation of both proton and deuteron correlation functions. It was demonstrated in [29] that the calculated pp phase shifts as obtained from both the delta-shell potential and the REID soft core potential [30]

agree well with the experimental data, up to about 150 MeV/c. As a cross check, the REID potential was also used to fit the experimental two-proton correlation function. The resulting correlation function is shown in Fig. 4 as the dashed line. The fitted radius parameter is  $3.05 \pm 0.02(\text{stat.}) \pm 0.24(\text{syst.})$  fm which, within errors, is consistent with the delta-shell potential calculation. The calculated two-proton correlation functions without Coulomb interaction and without any final state interactions are also shown in Fig. 4 as the dotted and dot-dashed lines, respectively.

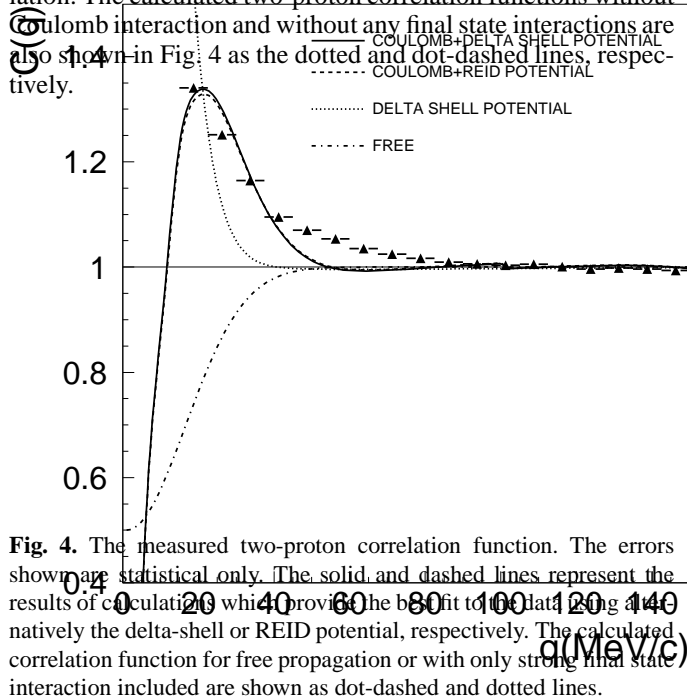


**Fig. 4.** The measured two-proton correlation function. The errors shown are statistical only. The solid and dashed lines represent the results of calculation which provide the best fit to the data, respectively the delta-shell or REID potential, respectively. The calculated correlation function for free propagation or with only strong final state interaction included are shown as dot-dashed and dotted lines.

In order to make a direct comparison with other experimental results, the CRAB package [27], provided by Pratt, was also used to extract the radius parameter for the two-proton system. The CRAB calculation takes into account the Coulomb and strong final state interactions. To describe the latter for the two-proton system the REID potential was taken. The measured momentum distribution of protons was used as input to the CRAB calculation. To obtain a radius parameter, the calculation was performed for a set of different radius parameters and then compared to the experimental data by calculating the  $\chi^2$  value. This gave a best fit radius parameter of  $2.83 \pm 0.20$  fm, that is consistent, within errors, with the delta-shell model calculation. The CRAB calculation result is shown in Fig. 5. The experimental correlation as a function of  $q_{inv}$  is also shown in Fig. 5 with the CRAB calculation. The solid and dashed lines represent the CRAB calculations with and without the experimental resolution effect included, respectively.

The polar angle (or rapidity) dependence of the proton source radius parameter was also investigated. Within errors, the two-proton source radius,  $R_0$  showed no rapidity dependence, as seen from Fig. 6, over the entire polar angle interval.

Two-proton correlations have also been studied in the target fragmentation region at the SPS in the WA80 experiment using the Plastic Ball spectrometer. Measurements were made with 200 A GeV proton, Oxygen, and Sulphur projectiles, on targets of C, Al, Ag, and Au [11]. The source radius extracted from the present analysis of the two-proton correlation for central Pb+Pb collisions at 158 A GeV is compared to the radius

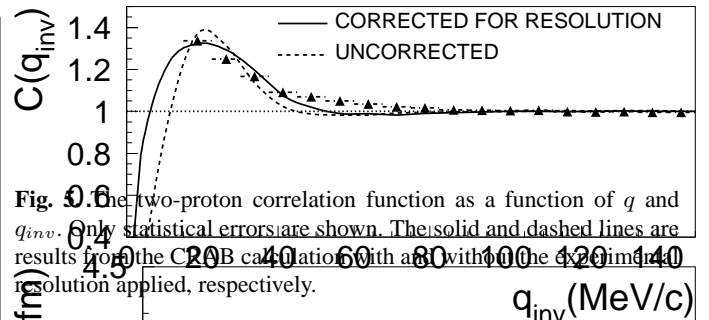
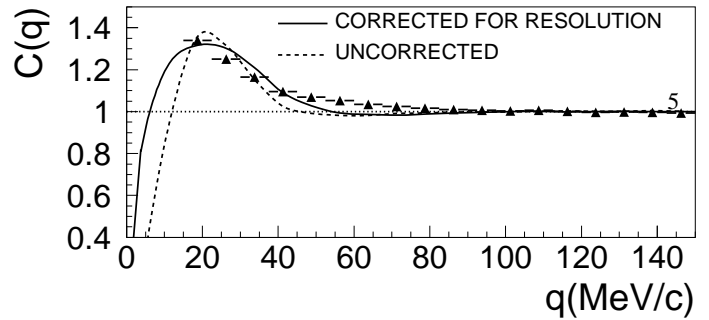


**Fig. 5.** The two-proton correlation function as a function of  $q$  and  $q_{inv}$ . Only statistical errors are shown. The solid and dashed lines are results from the CRAB calculation with and without the experimental resolution applied, respectively.

**Fig. 6.** Polar angle dependence of the proton-source radius parameters. The dashed line represents the weighted average.

parameters extracted in the WA80 experiment in Fig. 7. The radius parameters are plotted as a function of  $A_{Target}^{1/3}$ . All radii have been converted to root-mean-square radii. Within errors, the radius parameters measured in the WA80 and WA98 experiments at the SPS closely follow the target nuclear radius dependence of  $A_{Target}^{1/3}$  with little apparent dependence on the projectile mass. Since the size of the participant overlap region depends on both target and projectile mass, the observation of little projectile mass dependence indicates that the protons detected in the target fragmentation region are emitted from the entire target volume, following substantial rescattering [11].

### 3.4 Two-deuteron system

Figure 8 shows the measured two-deuteron correlation function and the theoretical calculation which gives the best fit to the data. The solid and dashed line represent the correlation functions calculated with final state interaction taken into account and that for free propagation. The fitted radius parameter is  $1.59 \pm 0.02(\text{stat.}) \pm 0.20(\text{syst.})$  fm. The range  $R$  and the strength  $s$  for the delta-shell potential are found to be  $0.52 \pm 0.01$  fm and  $1.08 \pm 0.01$ , respectively. The measured two-deuteron

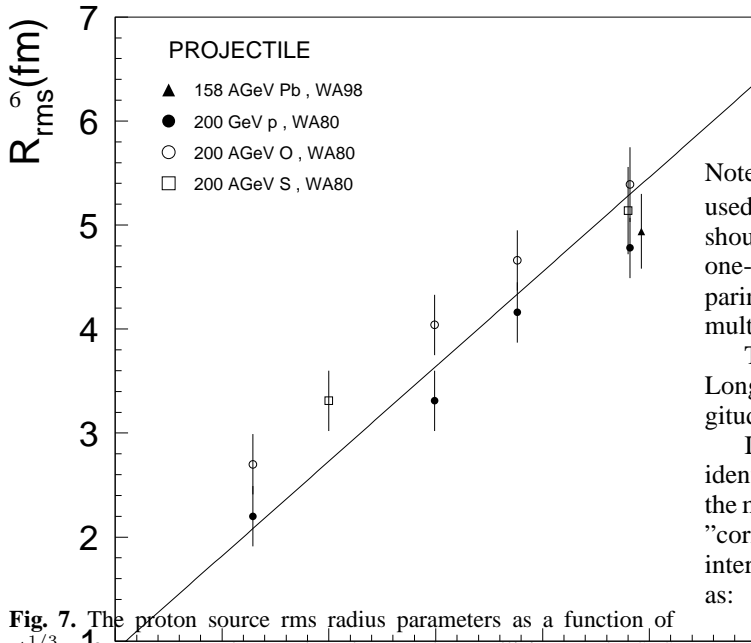


**Fig. 7.** The proton source rms radius parameters as a function of  $A_{\text{Target}}^{1/3}$  for proton-nucleus and nucleus-nucleus collisions at the SPS from this measurement and from the WA80 experiment [11]. The protons have been measured in the target fragmentation region with  $-0.6 < y < 0.6$  and  $100 \text{ MeV}/c < p_T < 650 \text{ MeV}/c$ . The symbols are slightly displaced for the Au and Pb target points for clarity. The line represents the fitted function  $R_{\text{rms}} = a A_{\text{Target}}^{1/3}$  ( $a = 0.91 \pm 0.02$ ,  $\chi^2/n = 1.68$ ). The WA80 experimental result was obtained using the CRAB code.

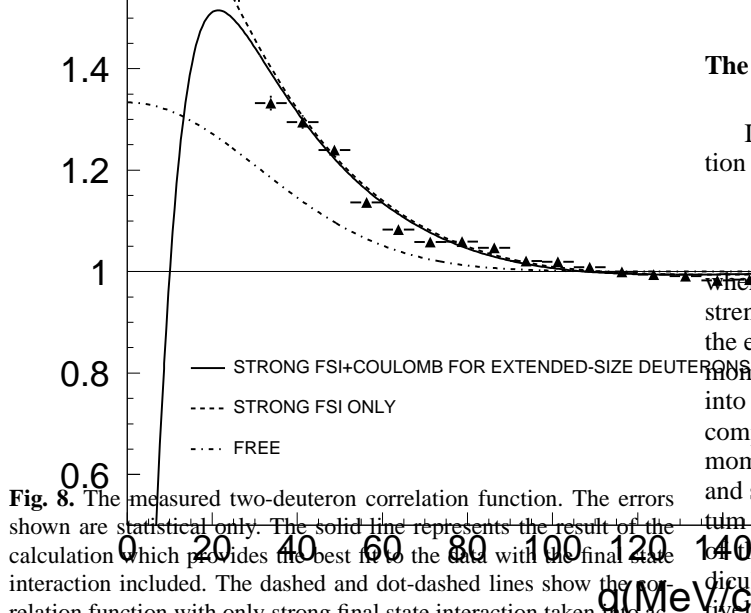


**Fig. 8.** The measured two-deuteron correlation function. The errors shown are statistical only. The solid line represents the result of the calculation which provides the best fit to the data with the final state interaction included. The dashed and dot-dashed lines show the correlation function with only strong final state interaction taken into account and that for free propagation, respectively.

correlation and extracted radius parameters show no dependence on the polar angle, similar to observations for the two-proton correlation (see Fig. 6).

## 4 Multi-dimensional analysis

For consistency of notation with previous analyses, the momentum difference  $\mathbf{Q} = (\mathbf{p}_1 - \mathbf{p}_2)$  is used in the multi-dimensional analysis. In this case the two-particle correlation  $C(Q)$  is given by:

$$C(Q) = 1 + \tilde{\rho}(Q)^2. \quad (8)$$

Note that since the correlation function  $C(q) = 1 + \tilde{\rho}(2q)^2$  was used for the calculations presented in section 3, a factor  $\sqrt{2}$  should be applied to the radius parameters obtained from the one-dimensional analysis results presented above when comparing with the radius parameters obtained from the following multi-dimensional analysis.

The multi-dimensional analysis has been performed in the Longitudinally CoMoving System (LCMS), in which the longitudinal pair momentum vanishes ( $\mathbf{p}_{z1} + \mathbf{p}_{z2} = 0$ ).

In order to extract that part of the correlation function of identical particles that is due to quantum statistical effects only, the measured multi-dimensional correlation functions have been "corrected" for the effect of the strong and Coulomb final state interactions (FSI). The corrected correlation function is defined as:

$$C(p_1, p_2) = K C_{\text{raw}}(p_1, p_2) \quad (9)$$

where  $K = C_{\text{FREE}}(Q)/C_{\text{FSI}}(Q)$  is the correction factor, and  $C_{\text{FREE}}(Q)$  and  $C_{\text{FSI}}(Q)$  are the calculated correlation functions for free propagation and with final state interactions included, respectively.

### 4.1 Two-proton system

#### The Bertsch-Pratt (BP) parametrization

In the Bertsch-Pratt parameterization [31,32], the correlation function for two fermions has the form:

$$C = N \left( 1 - \lambda e^{-Q_l^2 \cdot R_l^2 - Q_s^2 \cdot R_s^2 - Q_o^2 \cdot R_o^2 - 2 \cdot Q_o \cdot Q_l \cdot R_o^2} \right) \quad (10)$$

where  $N$  is the normalization constant and  $0 \leq \lambda \leq 1$  is the strength of the correlation which depends on the chaoticity of the emitter and on the purity of the measured data sample. The momentum difference vector  $\mathbf{Q}$  of two particles is decomposed into a longitudinal component along the beam axis ( $Q_l$ ) and a component transverse to the beam axis ( $Q_T$ ). The transverse momentum difference is further decomposed into the outward and sideward components. The outward and sideward momentum differences ( $Q_o$ ) and ( $Q_s$ ) are defined as the components of the transverse momentum difference parallel and perpendicular to the total transverse momentum of the pair, respectively. The sign convention is that  $Q_s$  is always positive,  $Q_l$  and  $Q_o$  are allowed to be positive or negative.  $R_o^2$  is the "out-longitudinal" cross term [33]. Its value can be either positive or negative. In the LCMS system the average resolutions in the  $Q_s$ ,  $Q_l$ , and  $Q_o$  components for the pp system are 20, 23, and 24 MeV/c, respectively.

Figure 9 shows projections of the measured two-proton correlation functions, corrected for final state interactions (Eq. (9)), onto the  $Q_l$ ,  $Q_s$ , and  $Q_o$  axes. Also shown are the corresponding projections of the fit of Eq. (10), shown as solid lines. The projected results and the fit results for a given  $Q$  component have been integrated up to 75 MeV/c over the other two  $|Q|$  components.

The parameters extracted from fits to the data using either the delta-shell corrected and CRAB corrected correlation functions are presented in Table 1. Also listed in this table are the

**Table 1.** Fitted parameters of the Bertsch-Pratt parametrization of the two-proton correlation function using the delta-shell model or CRAB model final state interaction calculations. Errors are statistical + systematic.

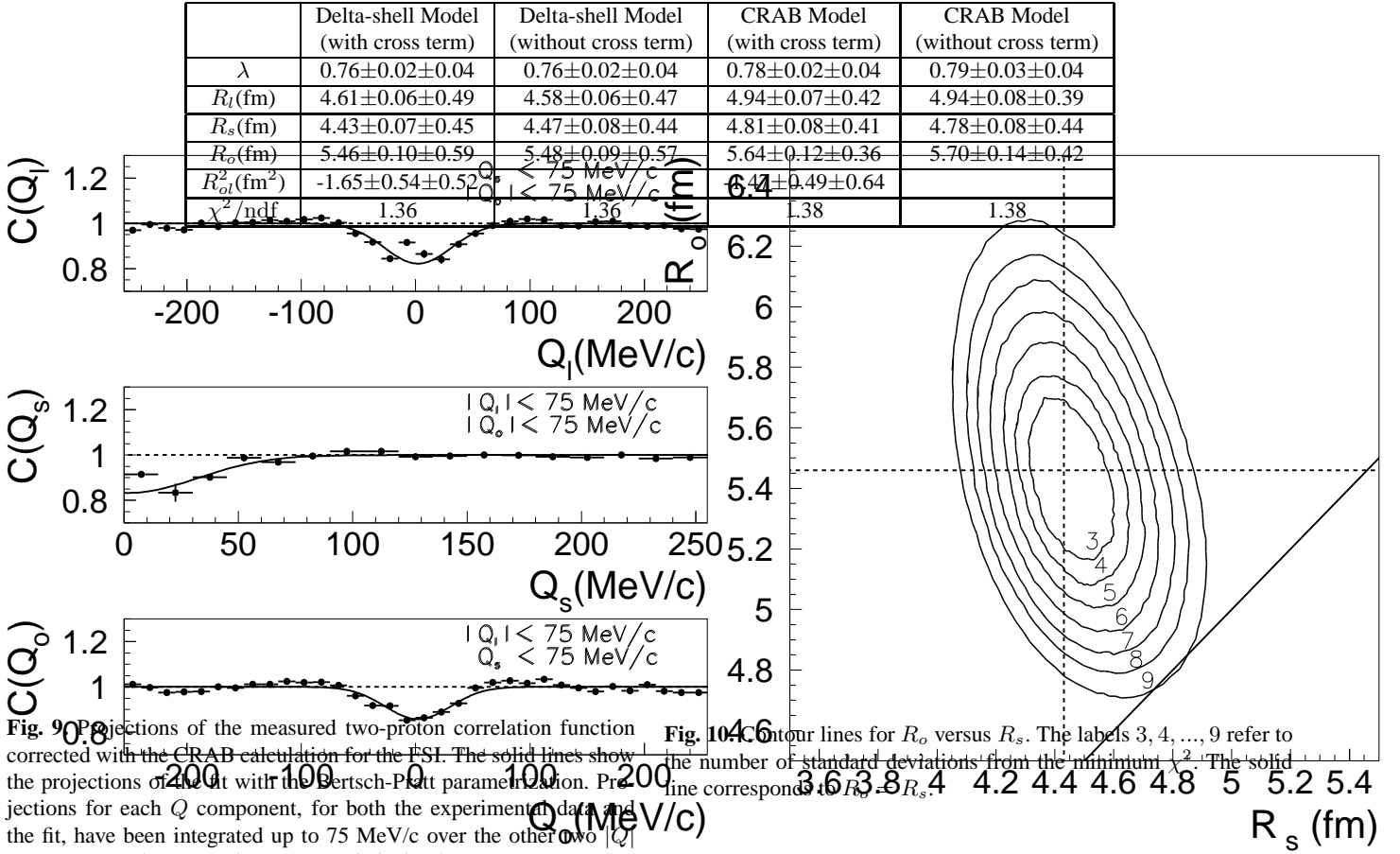


**Fig. 9.** Projections of the measured two-proton correlation function corrected with the CRAB calculation for the FSI. The solid lines show the projections of the fit with the Bertsch-Pratt parametrization. Projections for each  $Q$  component, for both the experimental data and the fit, have been integrated up to 75 MeV/c over the other two  $|Q|$  components. The errors shown are statistical only.

**Fig. 10.** Contour lines for  $R_o$  versus  $R_s$ . The labels 3, 4, ..., 9 refer to the number of standard deviations from the minimum  $\chi^2$ . The solid line corresponds to  $R_o = R_s$ .

fitted parameters without the cross term  $R_{ol}^2$ . Within errors, the delta-shell and CRAB corrections lead to the same values of fitted parameters. The fitted radius parameters with and without the cross term do not differ within errors. The cross term  $R_{ol}$  vanishes in the LCMS frame for longitudinally *boost-invariant* systems. The observation that the cross-term  $R_{ol}^2$  is small, indicates that the proton source undergoes an approximate boost invariant expansion.

The statistical significance of the fit is demonstrated in Fig. 10, where contour lines of equal confidence level for  $R_o$  versus  $R_s$  are plotted. The spacing of contours corresponds to one standard deviation in  $\chi^2$  value. The solid line, which represents equal sideward and outward radii, is 9 standard deviations from the minimum  $\chi^2$  value.

For transparent sources, where particles are emitted from throughout the entire volume, the longitudinal radius  $R_l$  is interpreted to measure the longitudinal size of the system directly, while the sideward radius provides a measurement of the transverse size. The duration of emission  $\Delta\tau$  is related [34,35] to the sideward radius  $R_s$  and outward radius  $R_o$  as:

$$\Delta\tau = \frac{1}{\beta_T} \sqrt{R_o^2 - R_s^2}, \quad (11)$$

where  $\beta_T$  is the transverse velocity of the particle pair. Notice that Eq. (11) is valid only when opacity effects and transverse flow are ignored. The excess of  $R_o$  over  $R_s$  is due to the duration of emission from the source in which particles with transverse velocity  $\beta_T$  travel a distance  $\beta_T \Delta\tau$  towards the detector, resulting in an apparent extension of the source in that direction. The sideward radius parameter  $R_s$  is not affected by the duration of emission since it is perpendicular to  $\beta_T$ .

Within errors, the radius parameters ( $R_l$ ,  $R_s$ ,  $R_o$ ) of the BP fit are quite close to each other (Table 1) which suggests a volume emission of the protons. The extracted  $R_o$  and  $R_s$  parameters, and the measured average value of  $\beta_T = 0.278 \pm 0.09$  for the proton pairs, gives  $11.5 \pm 2.5$  fm/c as an estimate of the emission duration.

In the case of a Bjorken scenario, with longitudinal expansion of the system without transverse flow, the  $m_T$  dependence of the longitudinal radius reflects the lifetime of the source[36]:

$$R_l = \tau_f (T_f/m_T)^{1/2}, \quad (12)$$

where  $T_f$  is the freeze-out temperature and  $m_T = \sqrt{m^2 + p_T^2}$ . Under the assumption that  $T_f = 120$  MeV, a source lifetime of about 13 fm/c is obtained.

Strictly speaking, the interpretation of  $\tau_f$  as the freeze-out time is based on the assumption that the longitudinal boost-invariant velocity profile existed not only at the time of freeze-out but also throughout the dynamical evolution of the reaction



zone. If this were not the case, then  $\tau_f$  would be larger. Hence,  $\tau_f$  estimated by Eq. (12) gives a *lower* limit for the lifetime of the source [1].

### The Yano-Koonin-Podgoretsky (YKP) parametrization

In the Yano-Koonin-Podgoretsky parameterization[37,38], the two-proton correlation function is defined by the formula:

$$C = N \left( 1 - \lambda e^{-Q_T^2 R_T^2 - (Q_l^2 - Q_0^2) R_l^2 - (Q \cdot U)^2 (R_0^2 + R_l^2)} \right) \quad (13)$$

where  $U = \gamma(1, 0, 0, \beta)$  is a 4-velocity with only a longitudinal component,  $\gamma = 1/\sqrt{1 - \beta^2}$ ,  $Q_T$  and  $Q_l$  are the components of the momentum difference projected onto the transverse and longitudinal directions, respectively,  $Q_0$  is the difference in energies. The sign convention is  $Q_0$  is always positive and  $Q_l$  can be either positive or negative. This parametrization has an advantage in that the three YKP radius parameters do not depend on the longitudinal velocity of the measurement frame, and the velocity  $\beta$  is closely related to the velocity of the effective particle emitter.

The parameters extracted from YKP fits to the delta-shell corrected or CRAB corrected correlation functions are listed in Table 2. Within errors, the fitted parameters obtained with the two different final state interaction corrections are consistent with each other.

**Table 2.** Fitted parameters of the YKP parametrization of the two-proton correlation functions using either the delta-shell model or CRAB model FSI corrections. Errors are statistical + systematic.

	Delta-shell Model	CRAB Model
$\lambda$	$0.75 \pm 0.04 \pm 0.04$	$0.77 \pm 0.03 \pm 0.03$
$R_l$ (fm)	$4.64 \pm 0.16 \pm 0.36$	$4.97 \pm 0.08 \pm 0.46$
$R_T$ (fm)	$4.42 \pm 0.13 \pm 0.40$	$4.73 \pm 0.06 \pm 0.46$
$R_0$ (fm)	$10.54 \pm 0.46 \pm 1.18$	$10.58 \pm 0.46 \pm 1.12$
$\beta$	$0.032 \pm 0.023 \pm 0.010$	$0.036 \pm 0.014 \pm 0.011$
$\chi^2/\text{ndf}$	1.42	1.47

Since the YKP velocity  $\beta$  is close to 0, it demonstrates that the LCMS frame coincides with the YK frame (the frame for which the YKP velocity parameter  $\beta$  vanishes). For *transparent sources*, and in the absence of flow, the radius parameters in the YK frame have a convenient physical interpretation.  $R_l$  and  $R_T$  are then interpreted as measures of the longitudinal and transverse size of the source, while  $R_0$  reflects directly the duration of emission from the source.

With similar fitted  $R_l$  and  $R_T$  parameters, and longitudinal velocity  $\beta$  compatible with 0, the YKP fit indicates a symmetric emission geometry with approximate boost invariant expansion of the source. The emission duration extracted from the YKP or BP fits are in agreement within errors.

The fitted YKP parameters are seen to be consistent with the BP parameters. Since the BP and YKP parametrizations are mathematically equivalent and differ only in the choice of independent components of  $q$ , the agreement between the two sets of fitted parameters serves additionally as a consistency check of the fitting procedures.

## 4.2 Two-deuteron system

### The Gaussian parametrization in the LCMS

Fig. 11 shows the experimental one-dimensional two-deuteron correlation function in the LCMS frame, after correction for final state interactions using the delta-shell model described in section 3. The correlation is fitted to the Gaussian correlation function:

$$C(Q) = N \left( 1 + \lambda e^{-Q^2 R^2} \right). \quad (14)$$

The fitted parameters are:  $\lambda = 0.43 \pm 0.03(\text{stat.}) \pm 0.08(\text{syst.})$ ,  $R = 2.50 \pm 0.10(\text{stat.}) \pm 0.28(\text{syst.})$  fm. The radius parameter is in agreement within errors with the radius ( $R = 1.59 \times \sqrt{2} = 2.25$  fm) extracted by fit to the one-dimensional correlation function with the full delta-shell model calculation (Fig. 8).

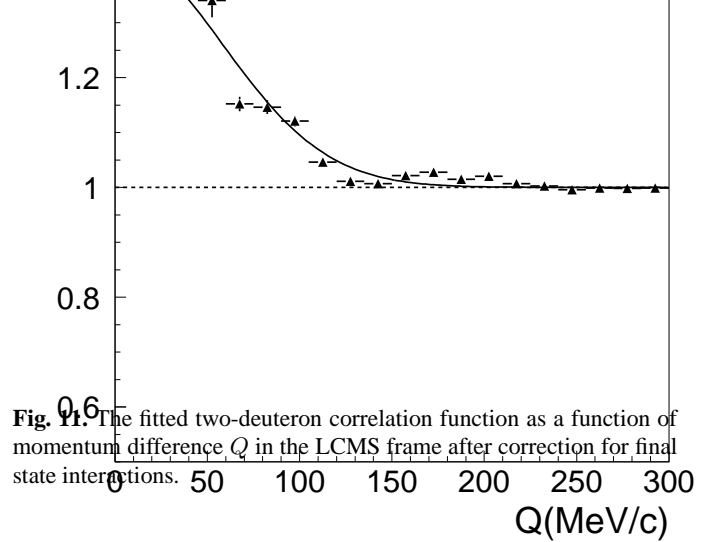


**Fig. 11.** The fitted two-deuteron correlation function as a function of momentum difference  $Q$  in the LCMS frame after correction for final state interactions.

### The Bertsch-Pratt parametrization

The two-deuteron correlation function has been corrected by the calculated delta-shell model two-deuteron final state interaction and fitted with the two-boson correlation function using the Bertsch-Pratt parametrization:

$$C = N \left( 1 + \lambda e^{-Q_l^2 R_l^2 - Q_s^2 R_s^2 - Q_o^2 R_o^2 - 2 \cdot Q_o Q_l R_{ol}^2} \right). \quad (15)$$

Projections of the measured two-deuteron correlation function on the  $Q_l$ ,  $Q_s$ , and  $Q_o$  axes are shown in Fig. 12. The measured and fitted projections in a given  $Q$  component have been integrated up to 75 MeV/c in the other two  $|Q|$  components. All  $Q$  components have approximately the same average resolution of 32 MeV/c.

The fitted parameters, with and without the cross term  $R_{ol}^2$ , are listed in Table 3. Within errors, the values of parameters extracted from the two different fits are the same. Similar to the result for the proton source, the small cross-term indicates that the deuteron source also experienced an approximate boost invariant expansion.

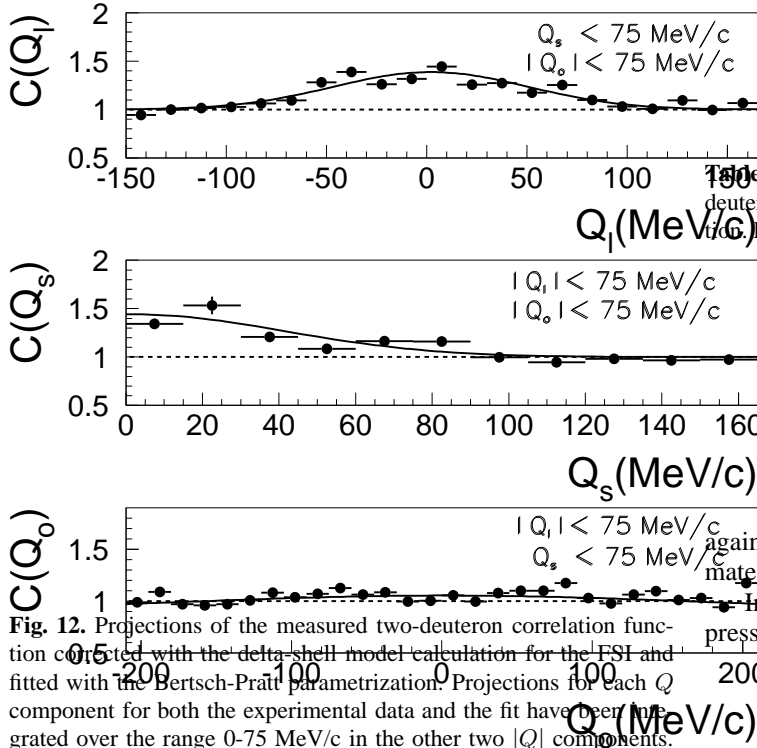


**Fig. 12.** Projections of the measured two-deuteron correlation function corrected with the delta-shell model calculation for the FSI and fitted with the Bertsch-Pratt parametrization. Projections for each  $Q$  component for both the experimental data and the fit have been integrated over the range 0-75 MeV/c in the other two  $|Q|$  components. The errors shown are statistical only.

**Table 3.** Fitted parameters of the Bertsch-Pratt parametrization of the two-deuteron correlation functions using the delta-shell model FSI correction. Errors are statistical + systematic.

	with cross term	without cross term
$\lambda$	$0.37 \pm 0.02 \pm 0.19$	$0.37 \pm 0.02 \pm 0.19$
$R_l$ (fm)	$2.17 \pm 0.10 \pm 0.24$	$2.13 \pm 0.08 \pm 0.18$
$R_s$ (fm)	$3.14 \pm 0.11 \pm 0.78$	$3.10 \pm 0.10 \pm 0.67$
$R_o$ (fm)	$0.01 \pm 0.08 \pm 0.02$	$0.01 \pm 0.04 \pm 0.03$
$R_{ol}^2$ (fm <sup>2</sup> )	$0.20 \pm 0.08 \pm 0.69$	
$\chi^2$ /ndf	1.52	1.52

Within errors, the fitted  $R_l$  and  $R_s$  parameters are close to the radius value obtained from the one-dimensional fit, while  $R_o$  is consistent with 0. For a transparent, azimuthally symmetric emission source, it is expected that  $R_s$  and  $R_o$  should be similar, except that  $R_o$  will be extended by the duration of emission, as discussed with respect to Eq. (11). The observation that  $R_o \ll R_s$  is inconsistent with such a transparent source, but may result naturally from surface emission from an opaque source [39,40]. Since deuterons are relatively large weakly bound objects, it might be expected that only those deuterons produced on the freeze-out surface via coalescence of an emitted proton and neutron survive. This would naturally lead to an opaque emission source, as observed.

### The Yano-Koonin-Podgoretsky parametrization

The two-boson correlation function in the Yano-Koonin-Podgoretsky parametrization is given by:

$$C = N \left( 1 + \lambda e^{-Q_T^2 R_T^2 - (Q_l^2 - Q_o^2) R_l^2 - (Q \cdot U)^2 (R_o^2 + R_l^2)} \right). \quad (16)$$

The parameters of the YKP fit to the two-deuteron correlation are listed in Table 4. The longitudinal velocity  $\beta$  is close to 0 indicating that the LCMS coincides with the YK frame and

**Table 4.** Fitted parameters of the YKP parametrization of the two-deuteron correlation functions using the delta-shell model FSI correction. Errors are statistical + systematic.

$\lambda$	$0.29 \pm 0.02 \pm 0.09$
$R_l$ (fm)	$1.29 \pm 0.07 \pm 0.42$
$R_T$ (fm)	$2.35 \pm 0.05 \pm 0.39$
$R_o^2$ (fm <sup>2</sup> )	$-46.95 \pm 1.69 \pm 8.82$
$\beta$	$0.020 \pm 0.002 \pm 0.007$
$\chi^2$ /ndf	1.42

again indicates that the deuteron source undergoes an approximate boost invariant expansion.

In the YK frame the YKP radius parameter  $R_0$  can be expressed as [41]:

$$R_0^2 = \frac{1}{\beta_\perp^2} (R_o^2 - R_s^2), \quad (17)$$

where  $\beta_\perp$  is the velocity of the particle pair transverse to the beam direction, and  $R_o$  and  $R_s$  are the outward and sideward radii of the BP parametrization. The negative value of  $R_0^2 \approx -47$  fm<sup>2</sup> obtained from the YKP fit is in agreement with the observation of strong opacity [1,39,42] of the deuteron source made in the previous section.

## 5 Discussion

Although one does not necessarily expect boost-invariance in the target fragmentation region at SPS energies, the small values of the cross-term  $R_{ol}$  in the BP parametrization as well as the consistency with zero longitudinal velocity  $\beta$  in the YKP parametrization of the correlation functions, indicates that both proton and deuteron sources exhibit boost-invariant expansion.

The measured one-dimensional radius parameter extracted for protons is markedly larger than that for deuterons. Comparison of the present results for protons and deuterons with those for  $\pi^+$ , also measured in the Plastic Ball [43], and  $\pi^-$  measured in the WA98 negative-charged particle spectrometer [44,45], and with  $K^+$  measured in the NA44 experiment [46] for central Pb+Pb collisions at 158 A GeV, reveals that the radii are observed so show a mass ordering with  $R_{\pi\pi} > R_{KK} > R_{pp} > R_{dd}$ . This observation is in agreement with previous reports [47] that lighter particles tend to give larger radius parameters. It is interesting that a large loosely bound composite object like the deuterons follows the same trend as observed for elementary particles. It has been shown by Alexander [47,48] that the source-size mass dependence of hadrons emerging from  $Z^0$  decays produced in  $e^+e^-$  annihilation can be reproduced using the Heisenberg uncertainty relations to derive the relations:

$$R = \frac{A}{\sqrt{m_T}}, \quad (18)$$

and

$$R_l = \frac{A}{\sqrt{m_T}}, \quad (19)$$

where  $A = c\sqrt{\hbar\Delta t}$  is a time scale constant,  $R_l$  is the longitudinal radius parameter, and  $m$  and  $m_T$  are the mass and the mean transverse mass, respectively. An alternative explanation using a QCD derived potential [47] proved to be equally successful. A different approach to explain the  $R$  and  $R_l$  mass dependence was given by Bialas and Zalewski [49,50,51]. In this description the radius parameter of the source is mass independent and its apparent decrease is a consequence of the momentum-position correlation expressed in the Bjorken-Gottfried condition [52,53]. However, a study of purely kinematical considerations [54] led to the conclusion that this is unlikely to account for the observed  $R(m)$  dependence.

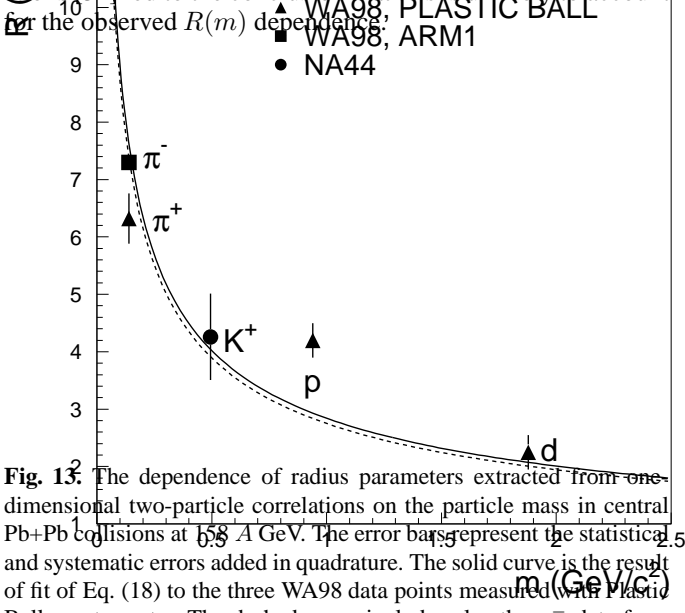


**Fig. 13.** The dependence of radius parameters extracted from one-dimensional two-particle correlations on the particle mass in central Pb+Pb collisions at 158 A GeV. The error bars represent the statistical and systematic errors added in quadrature. The solid curve is the result of fit of Eq. (18) to the three WA98 data points measured with Plastic Ball spectrometer. The dashed curve includes also the  $\pi^-$  data from WA98 and kaon data from the NA44 experiment.

Radius parameters extracted from one-dimensional two-particle correlation functions for central Pb+Pb collisions at 158 A GeV are shown as a function of the particle mass in Fig. 13. The  $\pi^- \pi^-$  radius parameter was measured with the negative-charged particle spectrometer of the WA98 experiment [44,45] and the two-kaon radius parameter was reported by the NA44 Collaboration [46], both measured near mid-rapidity ( $y$ )  $\sim$  2.9. In general, the radii follow the  $\sqrt{m}$  dependence expectation of Eq. (18). A fit of Eq. (18) to the  $\pi^+$  [43], proton, and deuteron radii measured with the WA98 Plastic Ball gives  $A = 2.84 \pm 0.13 \text{ fm GeV}^{1/2}$  with  $\chi^2/\text{ndf} = 12$ , as shown by the solid curve. This corresponds to a time scale of  $\Delta t = 40.8 \text{ fm/c}$  using the above expression for  $A$ , or to a freeze-out lifetime of  $\tau_f = 8.2 \text{ fm/c}$  using Eq. (12). A fit to all data points (dashed line) results in  $A = 2.75 \pm 0.04 \text{ fm GeV}^{1/2}$  with  $\chi^2/\text{ndf} = 7.2$ .

Previous results on pion and kaon interferometry for S+Pb and Pb+Pb reactions at the SPS have demonstrated scaling of the  $R_l$  and  $R_T$  radius parameters on the transverse mass,  $m_T$  [55,56]. The longitudinal and transverse radius parameters from the multi-dimensional YKP analysis of the two-proton and two-deuteron correlation functions are plotted as a function of the mean transverse mass in Figs. 14 and 15. Also shown are radius parameters for  $\pi^+$  measured with the Plastic Ball [43]. Radii measured near mid-rapidity for  $\pi^-$  in WA98 [44,45], and for kaons from the NA44 [56] and NA49 [57] experiments are also shown. The

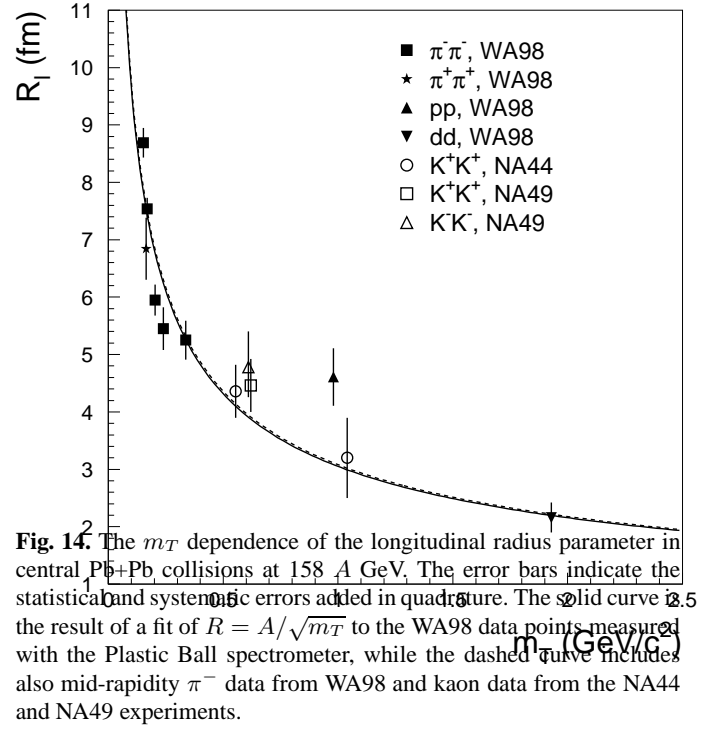


**Fig. 14.** The  $m_T$  dependence of the longitudinal radius parameter in central Pb+Pb collisions at 158 A GeV. The error bars indicate the statistical and systematic errors added in quadrature. The solid curve is the result of a fit of  $R = A/\sqrt{m_T}$  to the WA98 data points measured with the Plastic Ball spectrometer, while the dashed curve includes also mid-rapidity  $\pi^-$  data from WA98 and kaon data from the NA44 and NA49 experiments.

data are compared to fits of the form  $R_i = A_i/\sqrt{m_T}$ , where  $i = l, T$ . As can be seen from Figs. 14 and 15, within experimental uncertainties, the fitted  $R_l$  and  $R_T$  radius parameters are consistent with  $A/\sqrt{m_T}$  scaling. A fit to the three WA98 data points measured near mid-rapidity with the Plastic Ball spectrometer yields  $A_l = 3.05 \pm 0.17 \text{ fm GeV}^{1/2}$  with  $\chi^2/\text{ndf} = 3.6$ . When all data points are included in the fit, the fit yields  $A_l = 19.08 \pm 0.05 \text{ fm GeV}^{1/2}$  with  $\chi^2/\text{ndf} = 1.7$ .

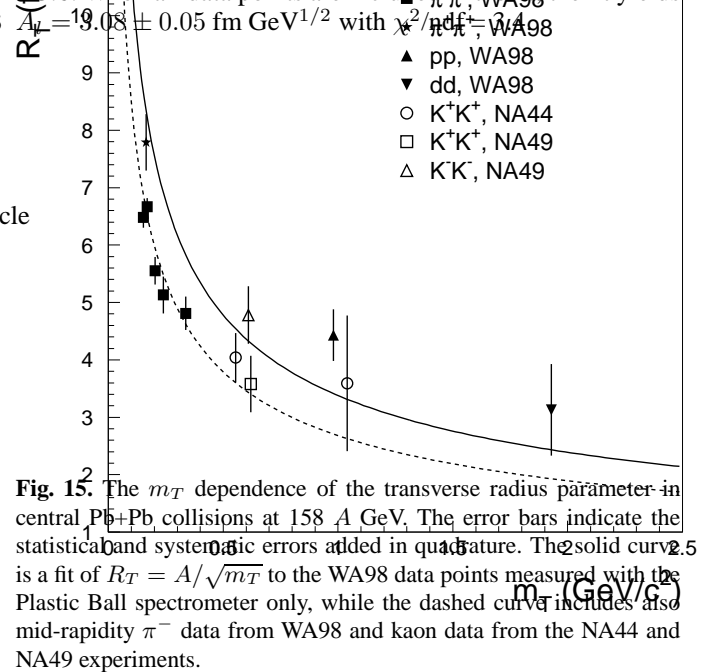


**Fig. 15.** The  $m_T$  dependence of the transverse radius parameter in central Pb+Pb collisions at 158 A GeV. The error bars indicate the statistical and systematic errors added in quadrature. The solid curve is a fit of  $R_T = A/\sqrt{m_T}$  to the WA98 data points measured with the Plastic Ball spectrometer only, while the dashed curve includes also mid-rapidity  $\pi^-$  data from WA98 and kaon data from the NA44 and NA49 experiments.

Although there is no theoretical justification to expect an  $R_T = A/\sqrt{m_T}$  dependence, the data are seen (Fig. 15) to follow such a dependence, within errors. A fit to the three WA98 data points measured near mid-rapidity with the Plastic Ball spectrometer yields  $A_T = 3.38 \pm 0.18 \text{ fm GeV}^{1/2}$  with  $\chi^2/\text{ndf} = 2.4$ . When all data points are included in the fit, the fit yields  $A_T = 2.68 \pm 0.04 \text{ fm GeV}^{1/2}$  with  $\chi^2/\text{ndf} = 3.3$ . A fit to the

pion and kaon data from NA44 experiment alone gave  $A_T = 3.0 \pm 0.2 \text{ fm GeV}^{1/2}$  [56].

## 6 Summary

In summary, we have measured two-proton and two-deuteron correlation functions in the target fragmentation region for central Pb+Pb collisions at 158  $A$  GeV.

In the one-dimensional analysis, the radius parameters were extracted from the measured correlations using calculations that assume a static Gaussian-shaped source. The extracted proton source radius parameter is about two times larger than that of the deuteron source. Comparison of the proton and deuteron radius parameters with those extracted from one-dimensional two-pion and two-kaon correlations reveals a common  $A/\sqrt{m}$  dependence with  $A \approx 3 \text{ fm GeV}^{1/2}$ . Such a dependence can be explained as a consequence of the Heisenberg uncertainty relations, under the assumption of a common duration of emission.

The multi-dimensional analysis demonstrates that the proton source exhibits a volume emission with long emission time, whereas the deuteron source is strongly opaque. The cross-term  $R_{ol}^2$  from the Bertsch-Pratt parametrization fit and the longitudinal velocity  $\beta$  from the Yano-Koonin-Podgoretsky parametrization fit are consistent with zero, suggesting that the proton and deuteron sources undergo an approximate longitudinal boost invariant expansion.

The longitudinal and transverse radius parameters,  $R_l$  and  $R_T$ , extracted from the multi-dimensional correlation analysis follow a common  $A/\sqrt{m_T}$  scaling for pions, kaons, protons, and deuterons, with  $A \approx 3 \text{ fm GeV}^{1/2}$  in both cases. The existence of a universal function describing the dependence of the radius parameters on the transverse mass for different particle species in the mass interval from pion to deuteron may indicate an approximately simultaneous freeze-out of the studied hadrons.

We wish to express our gratitude to Professor A. Deloff for supplying his codes for the pp and dd FSI calculations, and for his guidance and helpful discussions. We wish to thank the CERN accelerator division for the excellent performance of the SPS accelerator complex. We acknowledge with appreciation the effort of all engineers, technicians, and support staff who have participated in the construction of this experiment. This work was supported jointly by the German BMBF and DFG, the U.S. DOE, the Swedish NFR and FRN, the Dutch Stichting FOM, the Polish MEiN under Contract No. 1P03B02230 and CERN/88/2006 The Grant Agency of the Czech Republic under contract No. 202/95/0217, the Department of Atomic Energy, the Department of Science and Technology, the Council of Scientific and Industrial Research and the University Grants Commission of the Government of India, the Indo-FRG Exchange Program, the PPE division of CERN, the Swiss National Fund, the INTAS under Contract INTAS-97-0158, ORISE, Grant-in-Aid for Scientific Research (Specially Promoted Research & International Scientific Research) of the Ministry of Education, Science and Culture, the University of Tsukuba Special Research Projects, and the JSPS Research Fellowships for Young Scientists. ORNL is managed by UT-Battelle, LLC, for the U.S. DOE under contract DE-AC05-00OR22725. The MIT

group has been supported by the U.S. Dept. of Energy under the cooperative agreement DE-FC02-94ER40818.

## References

1. U.A. Wiedemann and U. Heinz, Phys. Rep. **319** (1999) 145 and references therein.
2. L.P. Csernai and J.I. Kapusta, Phys. Rep. **131** (1986) 223.
3. A. Pollieri et al., Phys. Lett. B **419** (1998) 19.
4. A. Pollieri et al., Phys. Lett. B **473** (2000) 193.
5. D. Fox et al., Phys. Rev. C **38** (1988) 146.
6. W.G. Gong et al., Phys. Rev. C **43** (1991) 1804.
7. D.A. Cebra et al., Phys. Lett. B **227** (1989) 336.
8. R. Kotte et al., Z. Phys. A **359** (1997) 47.
9. J. Bartke et al., Z. Phys. A **324** (1986) 471.
10. G.N. Agakishiev et al., Z. Phys. A **327** (1987) 443.
11. T.C. Awes et al., Z. Phys. C **65** (1995) 207.
12. H. Boggild et al., Phys. Lett. B **458** (1999) 181.
13. H. Appelshäuser et al., Phys. Lett. B **467** (1999) 21.
14. H.A. Gustafsson et al., Phys. Rev. Lett. **53** (1984) 544.
15. D.H. Boal et al., Rev. Mod. Phys. **62** (1990) 553.
16. Z. Chen et al., Phys. Rev. C **36** (1987) 2297.
17. J. Pochodzalla et al., Phys. Rev. C **35** (1987) 1695.
18. J. Pochodzalla et al., Phys. Lett. B **175** (1986) 275.
19. W.G. Lynch et al., Phys. Rev. Lett. **51** (1983) 1850.
20. T.C. Awes et al., Phys. Rev. Lett. **61** (1988) 2665.
21. C.B. Chitwood et al., Phys. Rev. Lett. **54** (1985) 302.
22. H. Gutbrod et al., *Proposal for a Large Hadron and Photon Spectrometer*, Report CERN/SPSLC 91-17, SPSLC/P260.
23. T.C. Awes et al., Nucl. Instr. Meth. A **279** (1989) 479.
24. G.R. Young et al., Nucl. Instr. Meth. A **279** (1989) 503.
25. A. Baden et al., Nucl. Instr. Meth. **203** (1982) 189.
26. R. Brun and F. Carminati, *GEANT Detector Description and Simulation Tool*, CERN Program Library, Long Writeup W5013.
27. S. Pratt <http://www.nsl.msu.edu/pratt/freecodes/crab/home.html>.
28. A. Deloff (unpublished).
29. A. Deloff, Phys. Rev. C **69** (2004) 035206.
30. B.D. Day, Phys. Rev. C **24** (1981) 1203.
31. S. Pratt, Phys. Rev. Lett. **53** (1984) 1219.
32. G. Bertsch et al., Phys. Rev. C **37** (1988) 1896.
33. S. Chapman et al., Phys. Rev. Lett. **74** (1995) 4400.
34. S. Pratt, Phys. Rev. D **33** (1986) 1314.
35. G. Bertsch and G.E. Brown, Phys. Rev. C **40** (1989) 1830.
36. A. Makhlin and Y.M. Synukov, Z. Phys. C **39** (1988) 69.
37. F. Yano and S. Koonin, Phys. Lett. B **78** (1978) 556.
38. M. Podgoretsky, Sov. J. Nucl. Phys. **37** (1983) 272.
39. H. Heiselberg and A.P. Vischer, Eur. Phys. J. C **1** (1998) 593.
40. S. Padula, Nucl. Phys. A **715** (2003) 637.
41. Y.F. Wu et al., Eur. Phys. J. C **1** (1998) 599.
42. B. Tomasik and U. Heinz, Eur. Phys. J. C **4** (1998) 327.
43. M.M. Aggarwal et al., WA98 Collaboration, unpublished.
44. M.M. Aggarwal et al., Eur. Phys. J. C **16** (2000) 445.
45. M.M. Aggarwal et al., Phys. Rev. C **67** (2003) 014906.
46. T. Kohama, PhD thesis, Hiroshima University, Jan., 2002.
47. G. Alexander et al., Phys. Lett. B **452** (1999) 159.
48. G. Alexander et al., Phys. Lett. B **506** (2001) 45.
49. A. Bialas and K. Zalewski, Acta Phys. Polon., B **30** (1999) 159.
50. A. Bialas et al., Phys. Rev. D **62** (2000) 114007.
51. A. Bialas et al., Acta Phys. Polon., B **32** (2001) 2901.
52. K. Gottfried, Phys. Rev. Lett. **32** (1974) 957.
53. J. D. Bjorken, Phys. Rev. D **7** (1973) 282.
54. M. Smith, Phys. Lett. B **477** (2000) 141.
55. I.G. Bearden et al., Phys. Rev. C **58** (1998) 1656; Eur. Phys. J. C **18** (2000) 317.
56. I.G. Bearden et al., Phys. Rev. Lett. **87** (2001) 112301.
57. S.V. Afanasiev et al., Nucl. Phys. A **715** (2003) 55.